Invited Paper

Compact holographic memory implemented with photorefractive crystals

George Barbastathis, Jean-Jacques P. Drolet†,
Ernest Chuang, and Demetri Psaltis

Department of Electrical Engineering
California Institute of Technology, MS 136-93, Pasadena, CA 91125
e-mail: {george,drolet,echuang,psaltis}@sunoptics.caltech.edu

† Current address: Holoplex, Inc.
600 S. Lake Ave., Pasadena, CA 91106

ABSTRACT

We have designed and implemented a compact holographic memory module that uses a dual spatial-light modulator / detector optoelectronic integrated circuit in the lens-less phase-conjugate geometry.[1] In this paper we discuss optical design and systems issues and present recent experimental results.

Keywords: holographic memories, photorefractive crystals, periodic hologram refreshing, liquid-crystal on silicon.

1 INTRODUCTION

Holographic storage[2] is appropriate for applications with high capacity and speed requirements. The data are stored as holograms recorded by the interference of a reference beam with a signal (data) beam. The reconstruction is obtained by illuminating the hologram by the reference beam alone. In three-dimensional media (as opposed to thin films), the Bragg selectivity effect makes it possible to multiplex holograms within the same volume by changing some property of the reference beam, for example the angle of incidence,[3,4] the wavelength,[5,6] the transverse phase encoding,[7] or the transverse location.[8] Thus the three-dimensional nature of the storage medium results in improved capacity by a factor roughly proportional to the number of superimposed holograms. The memory capacity is further increased by techniques which utilize the degeneracy properties of holograms.[9,10] Several of these multiplexing techniques or their combinations have been used recently in experimental demonstrations.[11–14]

Compared with commercial optical memories (e.g. digital video disks), holographic memories offer provably at least equal capacity,[14] and potentially both higher capacity and faster access time, by several orders of magnitude, but they also pose more stringent requirements on the quality of the recording and readout optical systems, and they take more space because of the bulky laser, optics, and vibration isolation equipment. It is therefore desirable to design holographic memories of physical size much smaller than currently available. Ideally, maximum

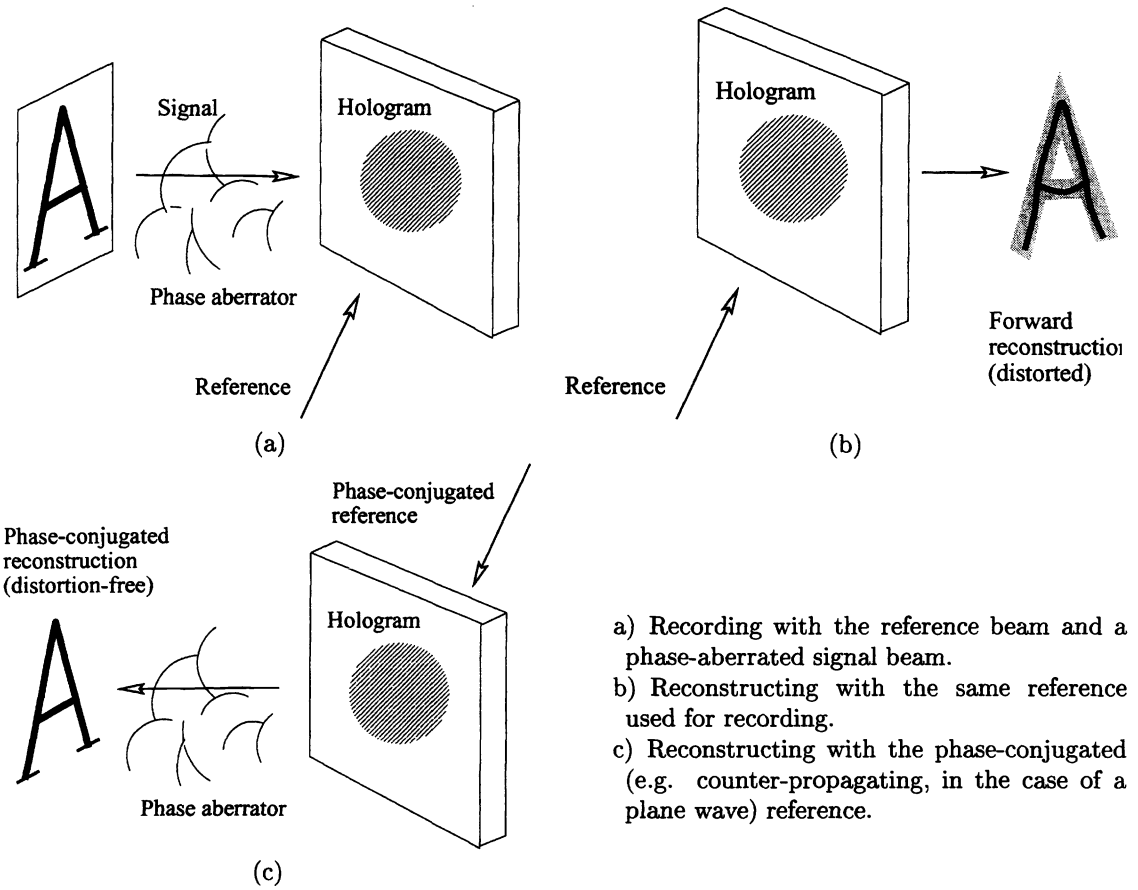

Figure 1: Obtaining distortion-free hologram reconstruction with a phase-conjugated reference.

robustness and compactness are achieved if the optical elements are placed close enough so that they can be glued to each other. Miniaturized optical sources (e.g. vertical-cavity surface-emitting lasers, VCSEL's) and components (beam-splitters, mirrors, waveplates) are readily available today, and optoelectronic technology is mature enough to provide reliable, high-performance integrated interfaces such as Spatial Light Modulators[15–17] (SLM's) and detector arrays. However, the imaging requirements[18–20] for high-capacity holographic storage usually force the designer to use expensive and bulky aberration-corrected lenses.[14] In this paper, we will use the well-known phase conjugation holographic technique[21–23] that allows wave-front distortion recovery without imaging in a properly designed architecture.

In a phase-conjugate system, distortion correction is obtained as follows[24]: suppose that a hologram is recorded by a reference beam R and a signal (object) beam $Se^{i\phi}$ (Fig. 1a), where S is the actual signal and ϕ is the phase aberration introduced by the beam propagation* (including Fresnel diffraction). The interference pattern is expressed as $\left|R + Se^{i\phi}\right|^2$. When R is used for reconstruction (Fig. 1b), $Se^{i\phi}$ is obtained on the signal axis as a continuation of the signal beam, carrying over all the phase aberrations introduced in the signal path during recording. Therefore the forward reconstruction is distorted and needs correction by using the appropriate imaging optics. If, however, the phase-conjugated reference R^* is used for reconstruction (Fig. 1c), the on-axis

*It is usually safe to ignore the effects of absorption on the phase-conjugation process.

reconstruction contains the term $S^*e^{-i\phi}$. The reciprocal aberrator introduces an additional phase term $e^{i\phi}$ to the counterpropagating reconstruction, and, as a result, a distortion-free intensity image $|S|^2$ is obtained at the location of the original signal.

The phase-conjugate reconstruction method has been used in the design of a refreshable dynamic holographic memory with liquid-crystal optoelectronic interface[1,25] as well as a read-only holographic memory with a conventional detector interface.[26] In both cases the motivation was to make the memory cheaper and more compact by eliminating the need for imaging optics. An additional motivation for refreshing architectures[1,27–30] is the decay of holograms in photorefractive materials during illumination or even in the dark; in silicon memories, leakage current through the output capacitors is the corresponding problem, and it is solved with a periodic read/re-write sequence, called refreshing. The dynamic compact memory architecture[1,25] befits a similar functionality.

In this paper we consider the implementation of a Tbit compact modular refreshable holographic memory in a volume comparable to that of a desktop personal computer. This corresponds to system volume density of several Tbits/m^3. To get an idea of the orders of magnitude involved, consider that the volume density of the Merriam-Webster dictionary is 60 Gbits/m^3, and the central Millikan Memorial Library at Caltech stores approximately 3 Tbits of information in 450,000 volumes. Therefore, our proposed system is capable of storing the contents of the entire library in a box smaller than a cubic meter!

We begin with the design of the basic compact memory module in section 2.1, and present experimental results from the laboratory implementation of the module in section 2.2. In section 3 we consider some of the basic issues in holographic memory design for our particular architecture, namely multiplexing method (section 3.1), system density optimization (section 3.2), and the trade-off between power, noise, error rate, and access time (section 3.3). Before concluding, we discuss some possible improvements in the architectures discussed so far in section 3.4.

2 COMPACT LENS-LESS HOLOGRAPHIC MEMORY ARCHITECTURE: BASIC MODULE

2.1 Structure of the basic module

The basic module used in dynamic compact holographic memories is shown in Figure 2. It consists of a photorefractive crystal, which acts as a re-writable holographic material, a polarizing beam-splitter, and an optoelectronic integrated circuit, the Dynamic Hologram Refresher[1,25,31] (DHR). The plane-wave reference beam is directly incident to the crystal through a liquid-crystal beam-steerer[32] for angle multiplexing. The signal beam is first deflected by the beam-splitter towards the optically active surface of the DHR die, where the signal information intensity-modulates the waveform. The modulated signal beam is reflected back to the photorefractive crystal where it records a hologram with the reference beam. The phase-conjugate method (see section 1) is employed for reconstruction. A counter-propagating reference beam passing through an identical beam-steerer (neither is visible in Fig. 2a) reconstructs the phase-conjugated signal which counter-propagates towards the DHR.

The counter-propagating beam may be provided by a mirror coating at the back face of the photorefractive crystal; in that case, the input beam must be steered at the complement of the desired readout angle. Yet another way to provide the phase-conjugate beam is by using a self-pumped phase conjugator in a separate crystal.[25] This solution is very elegant but it adds to the volume and cost of the basic module. In our experimental demonstration (next section) we used a Sagnac interferometer-like configuration to provide the phase-conjugated reference. In the theoretical derivations and volume optimization (section 3.2) we will assume that the mirror solution is used.

The surface of the DHR is organized as a grid of pixels, each containing a metal pad and a phototransistor.

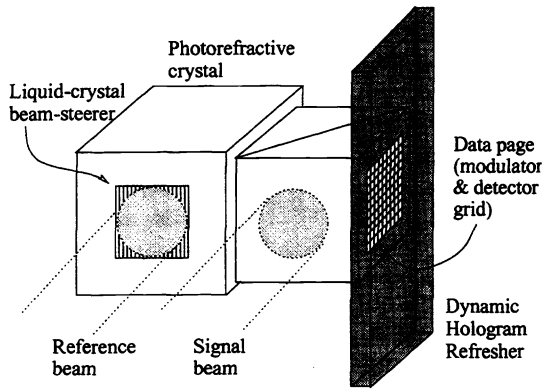

(a)

Entire pixel area	132 μm×211 μm
Active pixel area: (modulator)	49 μm×49 μm
(detector)	10 μm×10 μm
Number of pixels	20 × 24
Equivalent noise power	≤100 fWatts
Contrast ratio	18:1

(b)

Figure 2: (a) Basic module of a compact holographic memory. (b) Operation characteristics of the Dynamic Hologram Refresher.

A layer of hybrid-aligned nematic (HAN) liquid crystal is sandwiched between the silicon die and a transparent grounding electrode coated with indium-tin oxide (ITO). When a voltage is applied to the metal pad of a particular pixel, the phase of light incident to and reflected by the metal pad is modulated due to the electro-optic effect in the intervening liquid crystal.[17] Thus, with the aid of a polarizer, this device acts as an intensity modulator for each individual pixel.

The operating characteristics of the DHR are given in Figure 2b. The DHR functionality is three-fold:

(i) In the hologram recording phase, the DHR modulates incident light and reflects the modulated beam onto the photorefractive crystal, where a hologram is recorded by interfering with the reference.
(ii) In the hologram reconstruction phase, the diffracted beam obtained by the phase-conjugate method counterpropagates back onto the phototransistors, where the reconstructed pattern is detected by the DHR. Note that since the detectors are not collocated with the metal pad modulators, a truly phase-conjugated beam cannot be detected in the way we described so far. This problem is solved by introducing a small tilt in the reference beam along the degenerate direction, and has been proven to work in practice.[1]
(iii) In the hologram refreshing phase, the two previous operations are combined inside the DHR without external influence as follows: first the hologram is reconstructed by the phase-conjugated reference, detected as described in (ii), and latched in the internal memory of the DHR; then the detected pattern is transferred to the modulators and is used as signal to re-record a hologram with the forward reference thus reinforcing the original hologram.

The capacity of the basic module described so far is of the order of 1 Gbit, assuming that roughly 1,000 holograms can be stored in the photorefractive crystal, and each one contains approximately 1 Mbit (1000 × 1000 pixels). This goal is somewhat optimistic given the current state-of-the-art in integrated optoelectronic technology and holographic materials, however it is not far from being realizable.[31] We will pick up on this point in section 3.

2.2 Experimental results

The experimental setup used for testing the basic dynamic memory module is shown in Figure 3. Polarizing beam splitter PBS1 splits the input beam into two arms, the reference and signal. The reference is directed

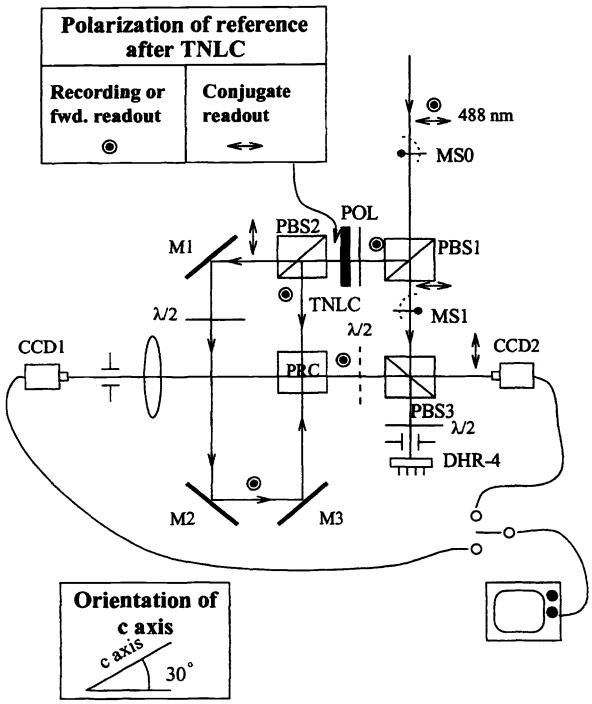

Figure 3: Experimental setup for testing the DHR module.

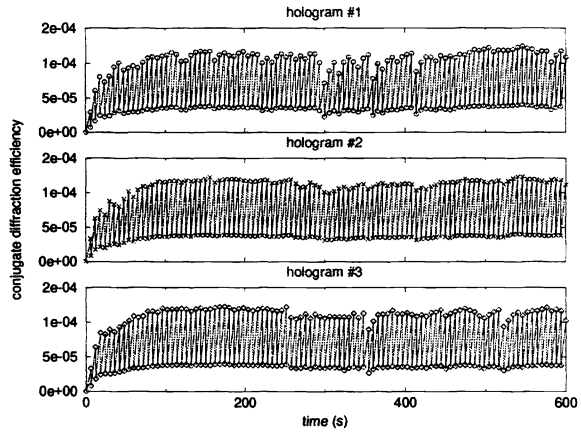

Figure 4: Sustainment of three holograms in the phase-conjugate reconstruction geometry, using the DHR chip.

into the Sagnac loop formed by PBS2 and mirrors M1, M2, M3. When the interferometer is aligned, the two counterpropagating beams are phase-conjugated. The signal, after passing through PBS3, is incident on the DHR where it gets modulated as described in section 2.1 before being reflected back towards the photorefractive crystal PRC, 30°-cut $BaTiO_3$ for this experiment. The arm of the reference beam reflected by PBS2 is used for recording, while the transmitted beam is used for phase-conjugate reconstruction. Mechanical rotation of the crystal in the plane of the figure is used to implement angle multiplexing. In addition to detecting the reconstruction on the DHR, we also used two CCD cameras to observe the both the forward and the phase-conjugated reconstruction for characterization purposes.

The operation of DHR as refresher with multiple holograms is shown in Fig. 4. In this experiment we stored three holograms and used the refreshing method described above to sustain and amplify them to saturation for 100 cycles. No errors were observed in any of the reconstructions. The probability of error, estimated from the pixel intensity statistics, was of the order of 10^{-3}. Sample images obtained by the DHR from the experimental setup of Fig. 3 are given in Figure 5. The calculated error probabilities for images a, b, c, d (please see caption) were 1.1×10^{-4}, 2.2×10^{-3}, 6.9×10^{-4}, 1.0×10^{-3} respectively. This shows not only that the phase-conjugated reconstruction is more reliable than the forward reconstruction (this was expected because of the self-correcting properties of phase-conjugation), but also that the deterioration resulting from multiple refreshing cycles is minimal. As of the writing of this paper, we have demonstrated up to 25 sustained holograms with similar performance.

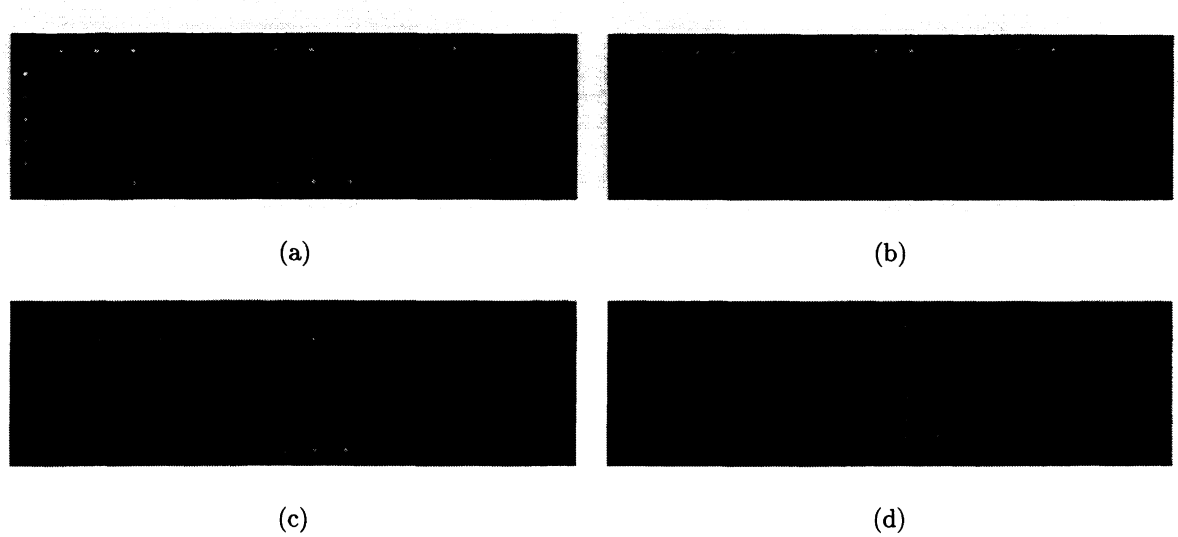

Figure 5: (a) DHR display; (b) reconstruction obtained with the forward reference, and conjugated reconstructions after (c) 1 and (d) 50 refreshing cycles.

3 ORGANIZATION OF THE MULTI-MODULE TERABIT HOLOGRAPHIC MEMORY

3.1 Multiplexing method

Angle multiplexing (along with fractal and peristrophic) has been widely used in high-capacity holographic memory demonstrations,[12–14,33] therefore it is the first candidate that comes to mind for the compact memory as well. The main challenge in the angle-multiplexing implementation is beam deflection. Since mechanical or acousto-optical deflectors are unacceptable, liquid-crystal beam-steerers[32] are a solution. Reflective liquid-crystal beam-steerers operating in the wavelength range of the final compact memory (670 nm, see section 3.2) are currently under development in our laboratory.

Alternative multiplexing methods alleviate the need for beam deflection, however they suffer from other disadvantages. More specifically:

1. wavelength multiplexing requires a tunable source over a broad spectral range in order to achieve high capacity;
2. phase-code multiplexing requires a Fourier-transforming system which would increase the volume; the Fourier transform may be omitted, but then phase-conjugation cannot be achieved with a simple mirror (the only way is a self-pumped phase-conjugator which would worsen the volume and optical power requirements of the system);
3. shift multiplexing is extremely difficult to achieve efficiently without mechanical translation.

Therefore it is clear that angle multiplexing with a reflective beam-steerer is the most practical solution, at least for the near future.

3.2 Optimization of the system volume

One of the advantages of the modular architecture described in the previous sections is that several of these modules may be combined in order to achieve high capacity. For example, if each module holds 1 Gbit (see section 2.1), then one may arrange 1,000 modules in a $10 \times 10 \times 10$ grid to obtain a Tbit memory. This calculation, however, is deceptively simple. During the high-capacity memory construction, several other issues must be taken into consideration, e.g. the location, number, and distribution of laser sources, power dissipation, mechanical stability, and system cost.[31] In this section we do a detailed optimization of the volume of the Tbit system versus certain design parameters, taking into consideration constraints imposed by technology.

The modular architecture that we consider in this paper is shown in Figure 6. The basic module is identical to the angle-multiplexed module of section 2, except with reflective liquid-crystal beam-steerer. The optics have been arranged carefully so that the spatial bandwidth is sufficient, i.e. that no significant amount of light is lost from any first-order diffraction beam, without wasting any extra space. Phase conjugation is achieved by means of a mirror coated on the crystal surface (not shown in the figures). Also, several waveplates (some of them implemented as liquid-crystal cells so that the phase rotation can be externally controlled) are in place to ensure the appropriate polarizations while maximizing the power efficiency of the system.

The active DHR surface contains $N \times N$ pixels, each one of size $b \times b$. The fill factor (which takes into account supporting circuitry surrounding the pixel metal pad) is ϕ, therefore the entire die area is $N^2 b^2/\phi^2$. The height of the DHR chip (perpendicular to the page level in Fig. 6b) is h. The beam diameter is L, and because of the special 90°-geometry arrangement, it is also equal to the hologram thickness, needed for the purpose of determining the Bragg selectivity. The sizes of the optical elements are $L_1 \times L_1$, $L_2 \times L_3$, and $L_4 \times L_4$ for polarizing beam splitter PBS1, photorefractive crystal, and PBS2, respectively. Additional lengths needed for the volume calculation are the integrated circuit thickness l_1, and the liquid-crystal variable waveplate thickness l_2.

The beam-steerer has angular resolution $\Delta\theta$ equal to the Bragg selectivity, which (in air) is given by $\Delta\theta = 2\lambda/L$ for 2nd-null separation, where λ is the wavelength in vacuum. The total angular swing allowed by the beam-steerer is θ in air. Because of Snell refraction, this angle is transformed into θ_g and θ_c inside the beam-splitter and crystal respectively (refractive indeces n_g, n_c). Therefore the number of holograms that can be stored inside the crystal in this architecture is

$$M = \frac{\theta_c}{\Delta\theta_c} = \frac{n_g \theta_g L}{2\lambda} \tag{1}$$

The signal beam undergoes appreciable Fresnel diffraction because of the small pixel size. The diffraction spreads χ_g, χ_c (in glass and crystal, respectively) are determined by scalar diffraction theory according to

$$\sin\chi_g = \frac{\lambda}{n_g b} \qquad \sin\chi_c = \frac{\lambda}{n_c b} \tag{2}$$

The sizes of the optical components can now be determined in terms of the DHR and beam-steerer parameters as follows:

$$L_1 = \frac{L}{1 - 2\tan\theta_g}, \tag{3}$$

$$L_2 = \frac{1}{1 - 4\tan\theta_c \tan\theta_g}\left(\frac{2L\tan\chi_c}{1 - 2\tan\theta_g} + \frac{Nb}{\phi(1 - 2\tan\chi_g)}\right), \tag{4}$$

$$L_3 = \frac{1}{1 - 4\tan\theta_c \tan\theta_g}\left(\frac{L}{1 - 2\tan\theta_g} + \frac{2Nb\tan\theta_c}{\phi(1 - 2\tan\chi_g)}\right), \tag{5}$$

$$L_4 = \frac{Nb}{\phi(1 - 2\tan\chi_g)}. \tag{6}$$

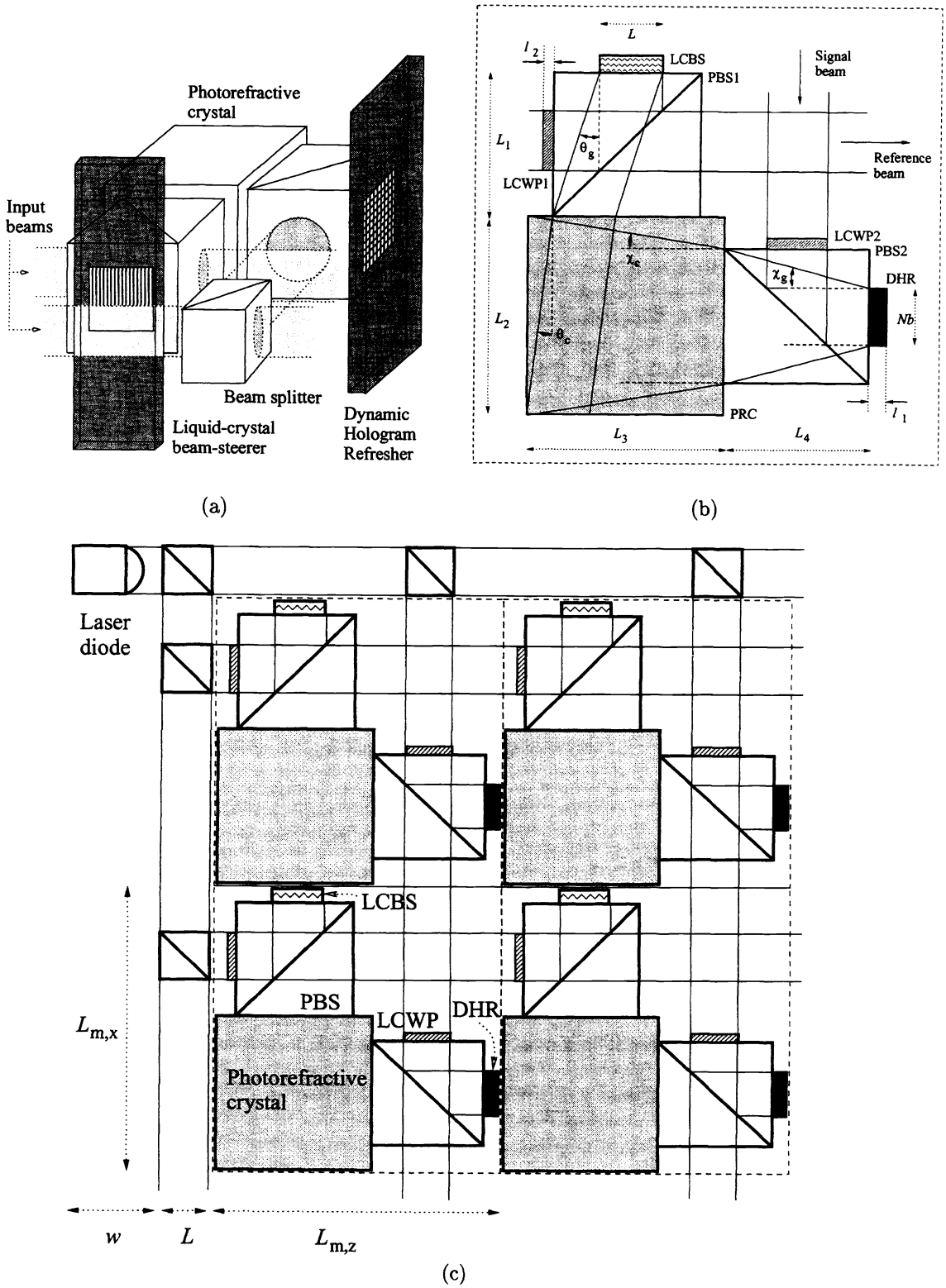

Figure 6: Schematic of the modular architecture. (a) Three-dimensional view of the basic module; (b) top view of the basic module; (c) arrangment of basic modules into a $G_x \times G_z$ (here 2×2) grid.

Let $L_{\mathrm{m},x}$, $L_{\mathrm{m},y}$, $L_{\mathrm{m},z}$ denote the dimensions of the basic module. From Figure 6b we obtain

$$L_{\mathrm{m},x} = l_1 + L_1 + L_2, \tag{7}$$

$$L_{\mathrm{m},y} = \max\{L_2\ ,\ h\}, \tag{8}$$

$$L_{\mathrm{m},z} = \begin{cases} l_1 + L_3 + L_4, & \text{if } l_2 < \dfrac{L_3 - L_1}{2}, \\ l_1 + l_2 + \dfrac{L_1 + L_3}{2} + L_4, & \text{otherwise.} \end{cases} \tag{9}$$

The modules are arranged in grids as shown in Figure 6c, each grid sharing the same laser diode (or VCSEL) source. The grid contains G_x basic modules in the x direction and G_z in the z direction (see figure). The density and access time would be higher in an arrangement with one source per basic module, because some excessive optical components (the peripheral beam-splitters delivering the beams to the modules in Fig. 6c) would not be required, and in addition it would be possible to read out each individual module simultaneously. However, source sharing alleviates problems due to excessive heat dissipation in the system, and also reduces the cost. Thus it seems that a small grid such as $G_x \times G_z = 2 \times 2$ is conservative enough for the heat and cost concerns without degrading the density and access time by much.

The grid volume is straightforward to calculate from Figure 6c. If we let w denote the size of the laser source, then

$$V_{\mathrm{grid}} = (L + G_x L_{\mathrm{m},x})\, L_{\mathrm{m},y}\, (w + L + G_z L_{\mathrm{m},z}) \tag{10}$$

The total number of (raw) bits that can be stored in the $G_x \times G_z$ grid is $G_x G_z M N^2$, therefore the volume density of the memory is

$$\mathcal{D} = \frac{G_x G_z M N^2}{V_{\mathrm{grid}}}. \tag{11}$$

This is our final result for the density. We seek to optimize $\mathcal{D}$ against the parameters N, b, θ, and L. Each one of them is constrained by technological limitations. A summary is given in the following table:

Parameter	Upper bound	value	Lower bound	value
Number of DHR pixels N	complexity of the circuitry	2000		1
DHR pixel size b	beam diameter L	1 cm	minimum feature size	4 μm
Beam diameter L	collimator aperture, active die size	1 cm	N/A	
Beam-steerer angular swing θ	minimum feature size	10° (in air)		0°

Parameter	Value
wavelength λ	670nm
refractive index n_g of glass	1.5
refractive index n_c of crystal	2.3
laser length w	5mm
integrated circuit thickness l_1	3mm
liquid crystal cell thickness l_2	1.5mm
DHR fill factor ϕ	0.5
grid size $G_x \times G_z$	2×2

Table 1: Parameters used for the density and volume calculations.

Parameter	Value
Number of DHR pixels N	1,250
DHR pixel size b	4 μm
Beam-steerer angular swing θ	10° (in air)
Laser beam diameter L	1cm
System density $\mathcal{D}$	36.0 Tbits m^{-3}
1 Tbit system volume	(30.3cm)^3
Number of grids and lasers N_g	123
Number of basic modules	492

Table 2: Results of density optimization.

The remaining parameters were considered fixed and are given in Table 1. It is instructive to calculate the required volume of a Tbit system constructed with our proposed architecture. Figure 7 shows the result versus N and b, obtained by fixing L and θ to their maximum values of 1cm and 10° respectively, and ignoring (for the moment) the technological limitations on N and b. As we observe, the volume is minimized for the optimal

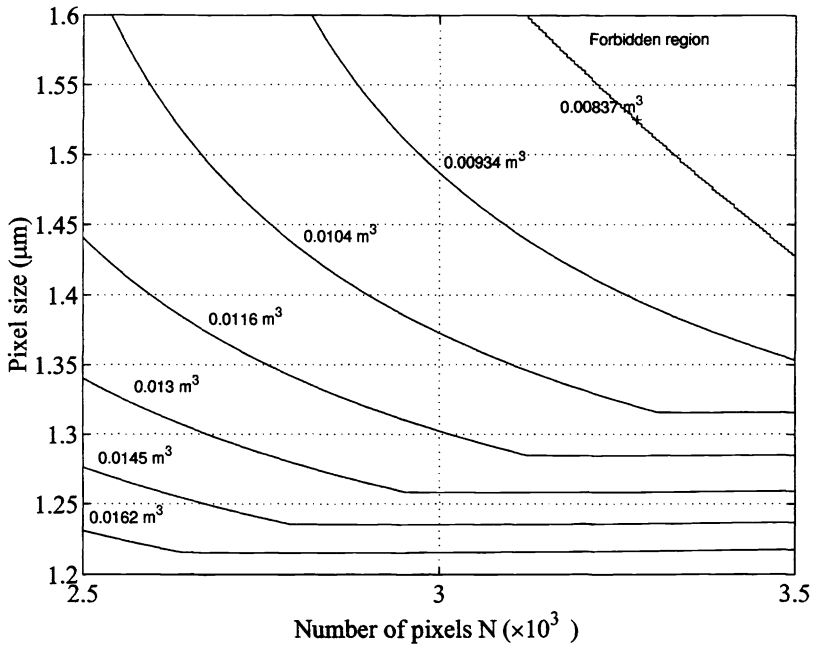

Figure 7: Volume of a Tbit modular memory constructed according to the architecture of Fig. 6 and the parameters of Table 1.

combination $N = 3,278$, $b = 1.53$ μm. The density at this point is 119.5 Tbits m^{-3}, and the system occupies a volume equivalent to that of a cube of dimension 20.3cm. If we increased b above its optimal value, then the overhead due to the diffraction spread would overcome the gain in density because of the larger allowable number of pixels, and hence the density would decrease. If, on the other hand, b increased to more than its optimal value, then $\mathcal{D}$ would again decrease, this time because N would decrease fast enough to overcome the reduced diffraction spread.

Unfortunately, the optimum found above is outside the feasible range of current technology. By solving the fully-constrained optimization problem, we find that it is best to fix b to its minimum value, θ and L to their maximum values, and set $N = \phi L/b$. The optimization results are given in Table 2.

3.3 Noise and data rate

The probability of error (PE, also known as bit-error rate) in the compact holographic memory (and any holographic storage system in general) is affected by two sources of noise: optical and electrical.[34,35] Optical noise inside a pixel is generated, for example, by light diffracted from neighboring pixels due to the finite modulation-transfer function of the optical system, by media scattering, laser speckle, etc. Electrical noise is generated by photoelectric current fluctuations, shot noise, etc. Let v denote the total electrical signal on the detector. Similar to previous work,[35] we model v as

$$v = v_{\text{opt}} + v_{\text{el}}, \tag{12}$$

where v_{opt} is the current generated by the optical signal (which contains only optical noise in the case of a dark – "OFF" – pixel, and mixture of signal plus noise in the case of a bright – "ON" – pixel) and v_{el} is the excess signal generated by electrical noise. We assume that the quantities v, v_{opt}, v_{el} are normalized to the intensity

variance of dark pixels σ_{dark}.

We now define the optical signal-to-noise ratio $(\text{SNR})_{\text{opt}}$ as

$$(\text{SNR})_{\text{opt}} = \frac{2\,(m_{\text{bright}} - m_{\text{dark}})}{\sigma_{\text{dark}}}, \tag{13}$$

where m_{bright}, m_{dark} are the mean optical intensities of bright and dark pixels respectively[†]. The probability distributions of v_{opt} for the dark and bright pixels are given respectively by

$$p_{\text{dark}}(v_{\text{opt}}) = \left(\frac{\mu}{2}\right)^{\mu} \frac{v_{\text{opt}}^{\mu-1}}{\Gamma(\mu)} \exp\left\{-\frac{\mu v_{\text{opt}}}{2}\right\}, \tag{14}$$

$$p_{\text{bright}}(v_{\text{opt}}) = \frac{1}{2}\left(\frac{v_{\text{opt}}}{\mu(\text{SNR})_{\text{opt}}}\right)^{\frac{\mu-1}{2}} \exp\left\{-\frac{v_{\text{opt}} + \mu(\text{SNR})_{\text{opt}}}{2}\right\} \text{I}_{\mu-1}\left(\sqrt{\mu(\text{SNR})_{\text{opt}} v_{\text{opt}}}\right), \tag{15}$$

where $\Gamma(.)$ is the Gamma function and $\text{I}_{\kappa}(.)$ is the modified Bessel function of 1st kind and order κ. The parameter μ appearing in the above equations is the effective degree of noise coherence. It can be calculated[‡] for the phase-conjugate architecture by using the van Cittert-Zernicke theorem[36] and is given by

$$\mu = \left(\frac{b}{4.88\lambda}\right)^2. \tag{16}$$

For the optimal $b = 4$ μm calculated above, we have $\mu = 1.5$.

The optical SNR is fixed by the properties of the optical system and the holographic material. For the data of Fig. 5d, using definition (13) we measured $(\text{SNR})_{\text{opt}} \approx 38.6$. We will consider this to be the upper limit on the optical noise performance.

The electrical SNR is defined as

$$(\text{SNR})_{\text{el}} = \frac{2\,(m_{\text{bright}} - m_{\text{dark}})}{\sigma_{\text{el}}}, \tag{17}$$

where σ_{el} is the variance of the electrical noise component. Because of the particular normalization of the electrical noise signal v_{el}, its approximate probability density function (independent of pixel value) is

$$p(v_{\text{el}}) = \frac{(\text{SNR})_{\text{el}}}{\sqrt{2\pi}(\text{SNR})_{\text{opt}}} \exp\left\{-\frac{v_{\text{el}}^2 (\text{SNR})_{\text{el}}^2}{2(\text{SNR})_{\text{opt}}^2}\right\} \tag{18}$$

The electrical SNR is determined by the noise behavior of the DHR circuit[31] and depends on the laser readout power P_{ref} and the detector integration time τ as

$$\left(\frac{(M/\#)^*\, L}{MN}\right)^2 P_{\text{ref}}\, \tau = 1.236 \times 10^{-7} \times (\text{SNR})_{\text{el}}^2 \left(1 + \sqrt{1 + \frac{5208}{(\text{SNR})_{\text{el}}^2}}\right), \tag{19}$$

where P_{ref} is expressed in mWatts, and τ in μsec. Here $(M/\#)^*$ is a system parameter that we call "specific M-number". It expresses the $(M/\#)$ system metric[37,38] for a holographic medium of unit-length. Since in the regime of weak holograms the diffraction efficiency increases with hologram thickness approximately as[39] L^2, the relation

$$(M/\#) = (M/\#)^*\, L \tag{20}$$

[†]A slightly different definition of SNR used often in optical systems is $(\text{SNR})_{\text{opt}} = \left(m_{\text{bright}} - m_{\text{dark}}\right) / \sqrt{\sigma_{\text{bright}}^2 + \sigma_{\text{dark}}^2}$. The two definitions are reconciled through the relation $\sigma_{\text{bright}}^2 = \sigma_{\text{dark}}^2 + 2\sigma_{\text{dark}}\left(m_{\text{bright}} - m_{\text{dark}}\right)$.

[‡]The complete calculation is beyond the scope of this paper.

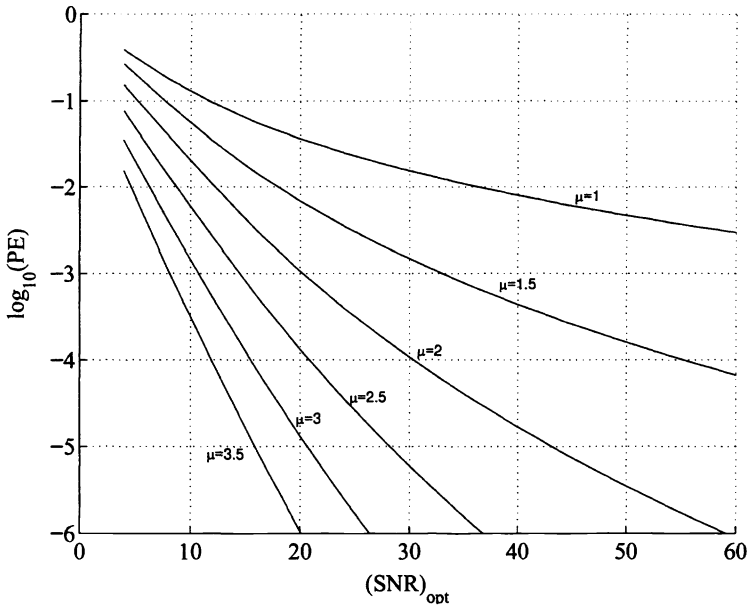

Figure 8: Probability of Error (PE) as function of optical signal to noise ratio $(\text{SNR})_{\text{opt}}$ for $(\text{SNR})_{\text{el}} = 10$ and different values of the noise coherence parameter μ.

provides a convenient means of expressing the effect of material thickness on the dynamic range of an otherwise invariant optical system.

The statistics of v are obtained by convolving $p(v_{\text{el}})$ with $p_{\text{dark}}(v_{\text{opt}})$ or $p_{\text{bright}}(v_{\text{opt}})$ for dark or bright pixels respectively. The probability of error PE is obtained by standard Bayesian estimation on the resulting distributions and depends only on the parameters $(\text{SNR})_{\text{opt}}$, $(\text{SNR})_{\text{el}}$, and μ. Numerical calculations indicate that reasonable PE can be obtained without severe losses in data rate if we use $(\text{SNR})_{\text{el}} = 10$. Some representative plots are given in Fig. 8.

We obtain the data rate by considering that only one module per grid may be read out at one time, but that all grids may be read out in parallel. The result is

$$\mathcal{R} = 32.3 \times \left(\frac{(M/\#)^* \lambda}{n_{\text{g}} \theta_{\text{g}} (\text{SNR})_{\text{el}}} \right)^2 \frac{N_g P_{\text{ref}}}{1 + \sqrt{1 + \dfrac{5208}{(\text{SNR})_{\text{el}}^2}}} \quad \left(\frac{\text{Gbits}}{\text{sec}} \right), \tag{21}$$

where N_g is the number of grids in the entire system, and the units are mm^{-1} for $(M/\#)^*$, μm for λ and mWatts for P_{ref}.

Thus for the optimal parameters given by Tables 1, 2, and with P_{ref}=120 mW, $(M/\#)^* = 0.25\ \text{mm}^{-1}$ we obtain $\mathcal{R} = 529.6$ Gbits/sec. However, from Fig. 8 we note that, for the chosen value of b ($b = 4\ \mu\text{m} \Rightarrow \mu = 1.5$), $(\text{SNR})_{\text{opt}}$ must be significantly high in order to achieve reasonably low PE. For example, if we set PE=10^{-4} as threshold, we would require $(\text{SNR})_{\text{opt}} \approx 55$. This is rather optimistic.

We can make the design more realistic by trading off some density for better error rate. From Fig. 8 we observe that $\mu = 2$ allows PE=10^{-4} to be achieved with only $(\text{SNR})_{\text{opt}} \approx 30$. By adjusting the values of b and N and re-computing density and data rate we obtain the final specifications of Table 3 (next page).

Parameter	Value	Parameter	Value
Number of DHR pixels N	1,081	System density $\mathcal{D}$	27.9 Tbits m^{-3}
DHR pixel size b	4.6 μm	1 Tbit system volume	$(33.0cm)^3$
Beam-steerer angular swing θ	10° (in air)	Number of grids and lasers N_g	164
Laser beam diameter L	1cm	Data rate $\mathcal{R}$	708.1 Gbits/sec

Table 3: Final design of 1 Tbit compact holographic memory.

Note that the above calculations refer to the *instantaneous* rather than the sustained data rate. They do not take into account the settling times for the liquid crystal devices, and the speed of the data bus connected to the DHR's.

3.4 Discussion

The cost of the basic dynamic memory module has been calculated and optimized versus current and projected industry standards in very similar architectures.[31] For our architecture, we estimate roughly $170 per module, therefore the cost of the optimized Tbit system[§] would be $112,000, or 89.6 cents/MByte. It turns out that the beam-steerer is a major component (approximately 50%) of the cost. We do hope that the reflective beam-steerer design will reduce this cost, thus making the entire system cheaper.

Several improvements may be made on the design we presented in section 3.2. For example, rather than the grid architecture of Figure 6c, one may use a linear architecture, where each laser is feeding a row of basic memory modules. This saves space because the peripheral beam splitters of Figure 6c that deliver the reference and signal beams to the modules would not be needed. A calculation along the lines of section 3.2 shows that the achievable density with the same parameters of Table 1 is 38.9 Tbits m^{-3}, in other words a memory of 1 Tbit would fit in a cube of dimension 29.5 cm. The data rate would be 608 Gbits/sec. The linear architecture does not have the nice property of equalized path lengths that we observe in Figure 6c. Therefore, a bulkier and/or more expensive source might be required for higher coherence, which would offset the density improvement.

Further improvement may be obtained by inserting a lens in the signal beam path, between DHR and PBS2, or between PBS2 and the storage crystal. This makes the optical system similar to the one proposed by van der Lugt[18] in 1975 for optimizing holographic storage. The lens may be of very poor quality, since the phase-conjugation process will undo all the aberrations it might induce in the signal beam. Therefore the volume taken by this lens, and the cost it adds to the system, would be immaterial. On the other hand, big gains are made in density and cost (since the volume of the photorefractive crystal would decrease) because the lens would reduce the signal beam spread. Our calculations[31] show that in most architectures the system volume density increases by $\sim 25\%$ and the cost is reduced by roughly $\sim 15\%$ when the lens is included. For lack of space we ommit the detailed analysis of this architecture in this paper.

Finally, one should mention that the analysis presented in section 3.2 contains several implicit approximations. For example, we did not take into account the effects on selectivity and diffraction efficiency of the displacement introduced to the phase-conjugate reference by the mirror coating. Several issues about the approximations will become clearer as the practical implementations progress further.

[§]The cost calculation does not include interfaces, packaging, or marketing.

4 CONCLUSIONS

We presented a modular holographic memory design capable of storing 1 Tbit in a volume of a ≈ 33 cm sized-cube, with an instantaneous data transfer rate of ≈ 700 Gbits/sec and raw error rate $\approx 10^{-4}$. Our laboratory implementation of the prototype module has proven in principle several aspects of our design, in particular the improved noise performance of the phase-conjugate readout, and the sustainment under illumination of multiple holograms inside the compact memory for a long time by means of periodic refreshing. Several technological improvements required to achieve the performance of our optimized design may be realistically expected within the next two-three years. In addition, several design improvements are also possible in order to make the Tbit holographic memory cheaper and denser.

Acknowledgments

This research was supported by the Defense Advanced Research Projects Agency and the National Science Foundation Center for Neuromorphic Systems Engineering at the California Institute of Technology. We are grateful to Greg Billock, Greg Steckman, Wenhai Liu, and Xu Wang for helpful discussions and to Yayun Liu for technical assistance.

References

[1] J.-J. P. Drolet, E. Chuang, G. Barbastathis, and D. Psaltis, "Compact, integrated dynamic holographic memory with refreshed holograms", *Opt. Lett.*, 22(8):552–554, 1997.

[2] P.J. van Heerden, "Theory of optical information storage in solids", *Appl. Opt.*, 2(4):393–400, 1963.

[3] E. N. Leith, A. Kozma, J. Upatnieks, J. Marks, and N. Massey, "Holographic data storage in three-dimensional media", *Appl. Opt.*, 5(8):1303–1311, 1966.

[4] D. L. Staebler, J. J. Amodei, and W. Philips, "Multiple storage of thick holograms in $LiNbO_3$", in *VII International Quantum Electronics Conference*, Montreal, 1972.

[5] G. A. Rakuljic, V. Levya, and A. Yariv, "Optical data storage by using orthogonal wavelength–multiplexed volume holograms", *Opt. Lett.*, 17(20):1471–1473, 1992.

[6] S. Yin, H. Zhou, F. Zhao, M. Wen, Y. Zang, J. Zhang, and F. T. S. Yu, "Wavelength–multiplexed holographic storage in a sensitive photorefractive crystal using a visible–light tunable diode–laser", *Opt. Commun.*, 101(5-6):317–321, 1993.

[7] C. Denz, G. Pauliat, and G. Roosen, "Volume hologram multiplexing using a deterministic phase encoding method", *Opt. Commun.*, 85:171–176, 1991.

[8] G. Barbastathis, M. Levene, and D. Psaltis, "Shift multiplexing with spherical reference waves", *Appl. Opt.*, 35:2403–2417, 1996.

[9] H. Lee, X.-G. Gu, and D. Psaltis, "Volume holographic interconnections with maximal capacity and minimal cross talk", *J. Appl. Phys.*, 65(6):2191–2194, 1989.

[10] K. Curtis, A. Pu, and D. Psaltis, "Method for holographic storage using peristrophic multiplexing", *Opt. Lett.*, 19(13):993–994, 1994.

[11] F. H. Mok, "Angle-multiplexed storage of 5000 holograms in lithium niobate", *Opt. Lett.*, 18(11):915–917, 1993.

[12] J. F. Heanue, M. C. Bashaw, and L. Hesselink, "Volume holographic storage and retrieval of digital data", *Science*, 265(5173):749–752, 1994.

[13] D. Psaltis and F. Mok, "Holographic memories", *Sci. Am.*, 273(5):70–76, 1995.

[14] A. Pu and D. Psaltis, "High density recording in photopolymer–based holographic 3D disks", *Appl. Opt.*, 35(14):2389–2398, 1996.

[15] D. A. Jared, R. Turner, and K. M. Johnson, "Electrically addressed spatial light modulator that uses a dynamic memory", *Opt. Lett.*, 16(22):1785–1787, 1991.

[16] D. A. Jared and K. M. Johnson, "Optically addressed thresholding very-large-scale-integration/liquid-crystal spatial light modulators", *Opt. Lett.*, 16(12):967–969, 1991.

[17] J. J. P. Drolet, J. S. Patel, K. G. Haritos, W. H. Xu, A. Scherer, and D. Psaltis, "Hybrid-aligned nematic liquid-crystal modulators fabricated on vlsi circuits", *Opt. Lett.*, 20(21):2222–2224, 1995.

[18] A. Vander Lugt, "Packing density in holographic systems", *Appl. Opt.*, 14(5):1081–1087, 1975.

[19] H.-Y. S. Li and D. Psaltis, "Three dimensional holographic disks", *Appl. Opt.*, 33(17):3764–3774, 1994.

[20] H.-Y. S. Li and D. Psaltis, "Alignement sensitivity of holographic 3-dimensional disks", *J. Opt. Soc. Am. A*, 12(9):1902–1912, 1995.

[21] A. Yariv, "Three-dimensional pictorial transmission in optical fibers", *Appl. Phys. Lett.*, 28:88, 1976.

[22] R. W. Hellwarth, "Generation of time-reversed wave fronts by nonlinear refraction", *J. Opt. Soc. Am.*, 67(1):1–3, 1977.

[23] R. A. Fischer, editor, *Optical Phase Conjugation*, Academic Press, 1983.

[24] A. Yariv, *Optical Electronics*, Sounders College, 4th edition, 1991.

[25] J.-J. P. Drolet, G. Barbastathis, and D. Psaltis, "Integrated optoelectronic interconnects using liquid-crystal-on silicon vlsi", in R. T. Chen and P. S. Guilfoyle, editors, *Optoelectronic interconnects and packaging*, volume CR-62, pages 106–131, 1996.

[26] Z. O. Feng and K. Sayano, "Compact read-only memory with lensless phase-conjugate holograms", *Opt. Lett.*, 21(16):1295–1297, 1996.

[27] Y. Qiao, D. Psaltis, C. Gu, J. Hong, P. Yeh, and R. R. Neurgaonkar, "Phase–locked sustainment of photorefractive holograms using phase conjugation", *J. Appl. Phys.*, 70(8):4646–4648, 1991.

[28] H. Sasaki, Y. Fainman, J. E. Ford, and S. H. Lee, "Dynamic photorefractive optical memory", *Opt. Let.*, 16(23):1874–1876, 1991.

[29] S. Boj, G. Pauliat, and G. Roosen, "Dynamic holographic memory showing readout, refreshing, and updating capabilities", *Opt. Let.*, 17(6):438–440, 1992.

[30] T. Dellwig, C. Denz, T. Rauch, and T. Tschudi, "Coherent refreshment and updating for dynamic photorefractive optical memories using phase conjugation", *Opt. Commun.*, 119:333–340, 1995.

[31] J.-J. P. Drolet, *Optoelectronic devices for information storage and processing*, PhD thesis, California Institute of Technology, 1997.

[32] D. P. Resler, D. S. Hobbs, R. C. Sharp, L. J. Friedman, and T. A. Dorschner, "High-efficiency liquid-crystal optical phased-array beam-steering", *Opt. Lett.*, 21(9):689–691, 1996.

[33] G. W. Burr, F. H. Mok, and D. Psaltis, "Angle and space multiplexed storage using the 90° geometry", *Opt. Commun.*, 117(1-2):49–55, 1995.

[34] C. Gu, G. Sornat, and J. Hong, "Bit-error rate and statistics of complex amplitude noise in holographic data storage", *Opt. Lett.*, 21(14):1070–1072, 1996.

[35] C. Gu, F. Dai, and J. Hong, "Statistics of both optical and electrical noise in digital volume holographic data storage", *Electr. Let.*, 32(15):1400–1402, 1996.

[36] J. W. Goodman, *Statistical Optics*, J. Wiley & Sons, 1985.

[37] D. Psaltis, D. Brady, and K. Wagner, "Adaptive optical networks using photorefractive crystals", *Appl. Opt.*, 27(9):1752–1759, 1988.

[38] F. Mok, G. W. Burr, and D. Psaltis, "A system metric for holographic memory systems", *Opt. Lett.*, 21(12):896–898, 1996.

[39] H. Kogelnik, "Coupled wave theory for thick hologram gratings", *Bell Syst. Tech. J.*, 48(9):2909–2947, 1969.